The Astrophysical Journal, 702:171–177, 2009 September 1 doi:10.1088/0004-637X/702/1/171

X-RAY SIGNATURE OF CHARGE EXCHANGE IN L-SHELL SULFUR IONS

M. Frankel[1], P. Beiersdorfer[1,2], G. V. Brown[1], M. F. Gu[1,2], R. L. Kelley[3], C. A. Kilbourne[3], and F. S. Porter[3]
[1] Lawrence Livermore National Laboratory, CA, 94550, USA; frankel4@llnl.gov
[2] University of California, Space Sciences Laboratory, Berkeley, CA, 94720, USA; beiersdorfer1@llnl.gov
[3] NASA/Goddard Space Flight Center, Greenbelt, MD, 20771, USA
Received 2009 April 17; accepted 2009 June 15; published 2009 August 10

ABSTRACT

The X-ray signature of L-shell charge exchange in sulfur was studied in the laboratory. A comparison of the charge exchange (CX) spectra with those obtained under electron-impact excitation showed marked differences. In the CX spectra, an enhancement was observed in the transitions from levels with high principal quantum numbers, $n = 4$, $5, 6 \rightarrow n = 2$ in comparison with the $n = 3 \rightarrow n = 2$ transitions that dominate the direct excitation spectra. An even greater enhancement was recorded in the transitions from the levels of electron capture to the ground states: $n = 7$, $8, 9 \rightarrow n = 2$. The spectra mainly consist of emission from S XIV, but lower charge states such as S XIII, S XII, and S XI also contribute. The results have been compared with observations made by the *Chandra* and *XMM-Newton* X-ray Observatories of Jupiter's polar regions. The enhancement we noticed in transitions from the high-n levels is not seen in the *Chandra* spectra.

Key words: atomic data – atomic processes – line: formation – line: identification – planets and satellites: individual (Jupiter) – X-rays: individual (Jupiter, laboratory)

Online-only material: color figure

1. INTRODUCTION

The origin of the soft X-ray emission from the Jovian polar regions has been a matter of speculation since its initial discovery, and an entirely satisfactory explanation for it has not yet been given. A measurement of the soft X-ray spectrum with the *Chandra X-ray Observatory* has shown two distinct peaks: one near 600 eV and the other near 300 eV (Elsner et al. 2005). This has also been confirmed by *XMM-Newton* observations (Branduardi-Raymont et al. 2004). The higher energy peak has been interpreted as arising from the emission of mainly helium-like oxygen, while the lower energy peak was attributed to the L-shell emission from the intermediate charge states of sulfur ions, or possibly the K-shell emission from carbon ions (Elsner et al. 2005). The oxygen, sulfur, and/or carbon ions are thought to precipitate in Jupiter's atmosphere so that much of the emission would be the result of charge exchange between the precipitating ions and the neutral gases in Jupiter's atmosphere. In this process, an electron (or more) is transferred from the neutral to the ion, leaving the ion in a highly excited state. This is followed by radiative decay.

The polar regions, from which the X rays are observed, have been mapped to the outer boundary of Jupiter's magnetosphere. Speculations have been made whether the ions are magnetospheric heavy ions residing in this area (Cravens et al. 2003) or solar wind heavy ions (Bhardwaj et al. 2007). In the magnetospheric case, charge-exchanging sulfur ions are thought to be responsible for the peak at 300 eV (Elsner et al. 2005). However, there is not enough phase-space density of energetic heavy sulfur ions to account for the measured X-ray intensity. For this reason it has been proposed that the ions are somehow accelerated to about 8 MeV (Cravens et al. 2003), so the phase-space distribution increases (Bhardwaj et al. 2007). If carbon is responsible for the emission, the ions should originate in the solar wind, since carbon and oxygen are the most abundant solar wind ions (Schwadron & Cravens 2000). These ions are thought to be accelerated to about 200 keV (Cravens et al. 2003) and then charge exchange with neutral gas in Jupiter's atmosphere (Elsner et al. 2005). It has also been proposed that both magnetospheric and solar wind heavy ions may contribute to the emission by magnetic reconnection near the cusp of Jupiter's magnetosphere (Bunce et al. 2004). However, a sulfur–oxygen plasma is, on many grounds, thought to be more likely than a carbon–oxygen plasma (Elsner et al. 2005; Cravens et al. 2003; Branduardi-Raymont et al. 2007; Kharchenko et al. 2006).

The CX emission from L-shell ions, including that from sulfur ions, is thought to contribute to the soft X-ray spectra of a variety of sources beyond Jupiter. For example, it is thought to be a major constituent of the C-band emission (around 1/4 keV) of comets and the Earth's magnetosphere (Kharchenko & Dalgarno 2001; Fujimoto et al. 2007), and it may contribute to the long-term enhancement of the soft X-ray background discovered in the *ROSAT* all-sky survey (Snowden et al. 1994; Cox 1998; Cravens 2000; Cravens et al. 2001). Moreover, some of the unidentified features observed with the Diffuse X-ray Spectrometer (Sanders et al. 2001) could potentially be due to lines produced by charge exchange involving L-shell ions, as could some of the lines in the spectrum of the soft X-ray background studied with the X-ray quantum calorimeter on a rocket flight (McCammon et al. 2002). Understanding the emission from L-shell ions is thus crucial to the interpretation of these spectra.

The K-shell X-ray emission from carbon and oxygen ions has been measured in the laboratory. However, little is known about the X-ray emission from L-shell ion in general, and L-shell sulfur ions in particular, which may play a role in producing the auroral emission on Jupiter and other sources inside and outside the solar system. For example, several measurements of K-shell CX emission were performed at the Electron Beam Ion Trap (EBIT) facility (Beiersdorfer et al. 2005b). Using EBIT laboratory data of CX-induced K-shell emission of carbon, nitrogen, and oxygen, Beiersdorfer et al. (2003) were the first to generate a fit in agreement with the X-ray spectrum of Comet Linear 1999 S4 based solely on CX, thereby validating

CX as a viable X-ray production mechanism. The K-shell-induced CX X-ray emission in heavy ions such as Fe XXV and Fe XXVI and Ar XVII has also been studied (Wargelin et al. 2005, 2008; Beiersdorfer et al. 2000, 2005a; Allen et al. 2005). The laboratory data have shown that updated, sophisticated models of CX-induced X-ray emission (Kharchenko & Dalgarno 2001; Kharchenko et al. 2003; Otranto et al. 2006; Perez et al. 2005) can still not fully reproduce many of the important features in the measured K-shell CX emission (Wargelin et al. 2005, 2008).

For L-shell CX-induced X-ray emission, the state of the art is even less developed than for the corresponding emission from K-shell ions, since only a few laboratory measurements exist, especially for high-Z ions. For example, moderate-resolution results from L-shell CX in iron have only recently been published (Beiersdorfer et al. 2008). The L-shell CX emission is significantly harder to model than the K-shell CX-induced X-ray emission. No detailed data—neither experimental, nor theoretical—exist for sulfur. In fact, it is very difficult to calculate the cross section of electron capture into anything but idealized levels. Most models use a one-electron approximation, i.e., the capturing ion is assumed to be bare, and the neutral gas is assumed to be atomic hydrogen (Olsen 1981). However, in L-shell ions the bound electrons' combined angular momentum couples to that of the captured electron resulting in a complex level structure that is not taken into account in these calculations. It is also difficult to predict the photon emission once a given level is occupied by CX. Even a simple helium-like ion has 1681 levels if all levels with a principal quantum number $n \leqslant 30$ are considered (Beiersdorfer et al. 2005a). The radiative cascade matrix connecting all of these levels is gigantic and generally truncated in models. Because of the need for approximations in the modeling, laboratory data are essential to guide the development of theory.

Here we present the first high-resolution X-ray spectra from open-shell sulfur ions as they recombine via charge exchange. The X-ray spectra are dominated by lithium-like sulfur. Since the high-resolution spectra of L-shell CX emission have not been seen before, the lithium-like system provides a stepping stone for more complex L-shell ions. However, lower charge states such as beryllium-like, boron-like, and carbon-like sulfur also contribute to the emission. Carbon-like sulfur is deemed to be the most important ion in the Jupiter auroral X-ray emission at 300 eV (Branduardi-Raymont et al. 2007). A comparison of our CX-produced spectra with those obtained under electron-impact excitation reveals a distinct pattern similar to that observed for K-shell spectra: A strong enhancement of the emission from levels with high principal quantum numbers is found. The measurements allow a first comparison with the Jovian spectrum, and we find that such an enhancement is not seen in the *Chandra* and *XMM* spectra. Instead, the Jovian spectra resemble more closely the laboratory spectra produced by electron-impact excitation. This supports suggestions that this particular emission may not come from sulfur CX. Further experiments carried out under conditions that better match the Jovian environment will be needed to corroborate these suggestions.

2. EXPERIMENTAL SETUP AND PROCEDURE

The measurements were carried out at the SuperEBIT electron beam ion trap facility at the Lawrence Livermore National Laboratory (Beiersdorfer 2008). SuperEBIT produces highly charged ions by shooting an electron beam through neutral gas, in our case sulfurhexafluoride, SF_6. The ions are trapped axially by the electron beam and confined radially by a magnetic field of 3T. Two different modes of SuperEBIT were used, the electron-trapping mode to ionize and excite the atoms, and the magnetic-trapping mode to let ions and neutral SF_6 gas recombine through charge exchange (Beiersdorfer et al. 1996). In the electron-trapping mode the electron beam was on. It ionized and excited the injected gas molecules until the equilibrium charge state distribution was reached. The X rays during the electron-trapping mode are mainly produced by electron-impact excitation. We used a beam energy of 3.09 keV, chosen to produce a charge balance dominated by S^{14+} ions. The energy was thus high enough to ionize S^{13+} but too low to ionize S^{14+}. However, the beam energy only determines the maximum charge state. There were also some S^{13+}, S^{12+}, and S^{11+} ions present in the trap. By monitoring the amount of helium-like ions created as a function of time, we could pinpoint the necessary amount of time needed to produce the desired charge state. This was at about 0.59 s. After 0.59 s, the number of counts in the resonance line $1s2p\ ^1P_1 - 1s^2\ ^1S_0$ in S^{14+} was not increasing significantly.

After producing the ions, the magnetic mode was entered. The radial trapping during the magnetic mode was accomplished by the 3T magnetic field of SuperEBIT. The electron beam was turned off and the highly charged sulfur ions (S^{14+}) were left to interact with neutral gas for 0.94 s. This time was sufficient for the CX to occur, but short enough to allow for a good duty cycle. Since there is no electron beam in the magnetic mode to reionize the sulfur ions, the prevailing helium-like sulfur ions only recombine once to produce the desired lithium-like spectrum. The helium-like ions were thus destroyed in the process, and could not be reionized as they would be in direct excitation. Hence, CX spectra in EBIT are a lot weaker than direct excitation spectra. The data were collected during four run days.

The trap was opened once every cycle by dropping the voltage of the top drift tube. The ions could then exit the trap axially and a new timing cycle would begin. Purging the trap and refilling it with new sulfur ions is a way of hindering unwanted species, such as barium or tungsten, from accumulating in the trap and contaminate the spectra (Marrs 2008).

The X-ray emission was monitored with the EBIT Calorimeter Spectrometer (ECS). The ECS covers a large range of X-ray energies, about 0.1–100 keV. The resolution is better than 5 eV at 400 eV, which is the approximate energy for the $n = 3 \rightarrow n = 2$ lines in S XIV (Porter et al. 2008). However, there is some X-ray absorption by four infrared blocking filters in the microcalorimeter, which are used as thermal shields. The absorption of a combined 1434 Å of aluminum and 2182 Å of polyamide is especially high at low energies. Since we wanted to record the rather low-energy sulfur X-ray emission between about 300 and 700 eV, we deliberately equipped the ECS with such thin filters. The response function of these filters has to be kept in mind when comparing lines across the spectrum. Figure 1 shows the total response function of the ECS.

3. RESULTS

The results of the measurements are displayed in Figures 2–4. The individual transitions in each charge state have been identified using the spectral data from high-resolution grating-spectrometer measurements of the emission lines of L-shell sulfur (Lepson et al. 2005). To calculate the transition energies of the lines emanating from high principal quantum numbers, an atomic structure code called the General Relativistic Atomic

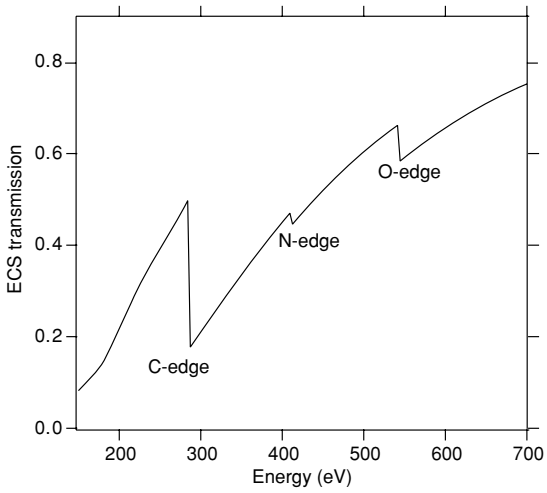

Figure 1. ECS quantum efficiency in the energy range of our measurement using data from the Center for X-ray Optics (www-cxro.lbl.gov) appropriate for the thicknesses and composition of the four infrared blocking filters.

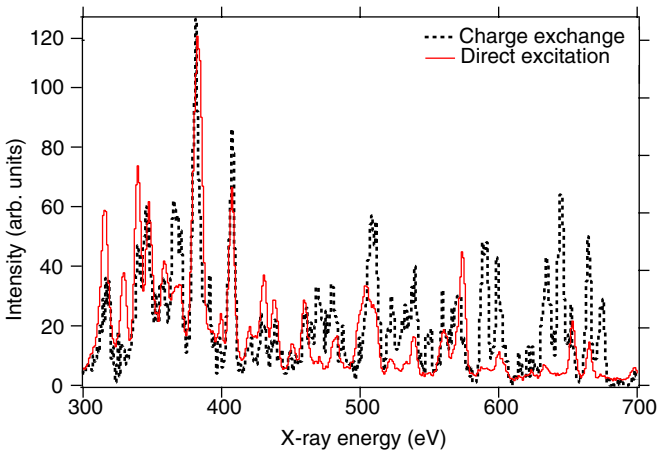

Figure 2. Comparison of the S XIV X-ray spectra produced by direct excitation and CX at an electron beam energy of 3.09 keV.

(A color version of this figure is available in the online journal.)

Structure Package (GRASP) was used (Parpia et al. 1996). These calculations helped in the identification of the lines that had not been previously measured. All the identified transitions are listed in Tables 1–4.

3.1. Collisional Spectra

Oxygen and nitrogen are natural background constituents in SuperEBIT. The strong lines they give rise to in the direct excitation spectra are the features labeled O z, O y, O w, and O Kβ from He-like oxygen, O Lyα and O Lyβ from hydrogen-like oxygen, N z and N w from helium-like nitrogen, and N Lyα and N Lyβ from hydrogen-like nitrogen. They have been observed in our spectra and are listed in Tables 1–4. The spectra also contain some K-shell fluorine peaks, since we used SF_6 gas. However, these lines are above 700 eV and did not interfere with the lines of our interest between 300 and 700 eV.

The direct excitation spectrum of sulfur from the electron-trapping mode is dominated by the $n = 3 \rightarrow n = 2$ transitions. In the lithium-like sulfur (S XIV) spectrum, these lines are from $3d \rightarrow 2p$, $3p \rightarrow 2s$, and $3s \rightarrow 2p$ transitions in order of decreasing intensity, as can be seen in Figure 2. The lines are found between 369 eV and 407 eV. The $n = 4,5 \rightarrow n = 2$ transitions in S XIV are a lot weaker and blended with other lines. In Figure 3 one can see the $n = 4 \rightarrow n = 2$ and $n = 5 \rightarrow n = 2$ transitions at around 507 eV and 570 eV, respectively. The $n = 4 \rightarrow n = 2$ transitions are blended with S XIII-lines, and the $n = 5 \rightarrow n = 2$ peaks are blended with Oxygen (O y). There are no higher n transitions readily visible in the direct-excitation spectrum of S XIV or any of the other charge states.

3.2. Charge Exchange Spectra

As expected for a spectrum produced by direct excitation, the intensities of the peaks decrease as a function of n for all charge states. This is not true for the CX spectrum. In the CX spectrum of S XIV, the $n = 4, 5, 6 \rightarrow n = 2$ transitions are enhanced relative to the $n = 3 \rightarrow n = 2$ transitions. There is an even greater enhancement in the $n_c = 7, 8, 9 \rightarrow n = 2$ transitions, where n_c is the principal quantum number into which the electron is captured in the CX collision. Figure 2 shows an overlay of spectra produced by CX and direct excitation, whereas Figures 4 and 3 show the spectra produced by CX and direct excitation separately.

The strongest S XIV-line among these high-n transitions is the line feature labeled S XIV-13 in Figure 4. It is a blend of the $9s \rightarrow 2p$ and the $9d \rightarrow 2p$ transitions due to electron capture and can be found at 644 eV. In the overlaid spectrum in Figure 2, one can see that this line is greatly enhanced in the CX

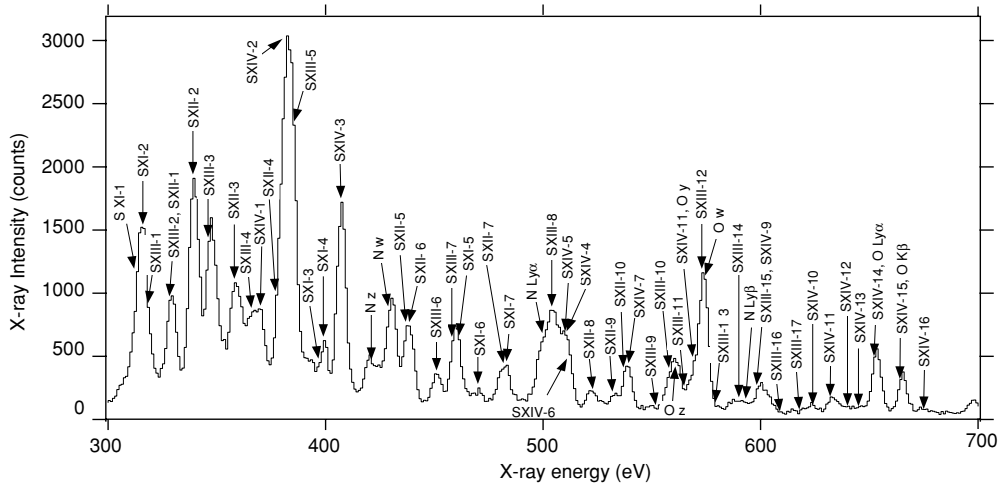

Figure 3. X-ray spectrum produced by direct excitation at an electron beam energy of 3.09 keV. The lines are labeled using the notation of Tables 1–4.

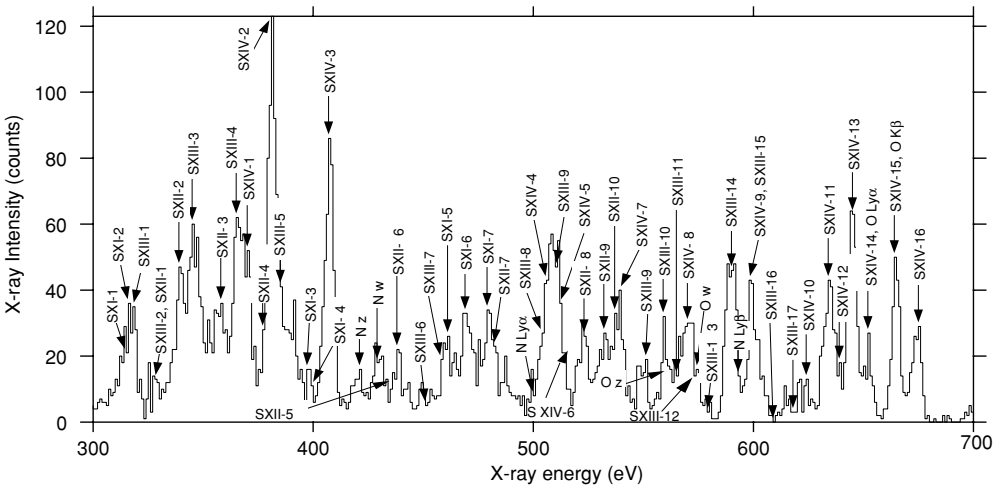

Figure 4. X-ray spectrum produced by CX electron beam off. The lines are labeled using the notation of Tables 1–4.

Table 1
Identified Transitions

Line/blend	Energy (eV)	Transition
S XI-1	314.5[a]	$(1s^2\ 2s^2\ 2p_{3/2}\ 3d_{5/2})_3 \rightarrow (1s^2\ 2s^2\ 2p^2_{3/2})_2$
S XI-1	315.0[a]	$(1s^2\ 2s^2\ 2p_{3/2}\ 3d_{5/2})_2 \rightarrow (1s^2\ 2s^2\ 2p^2_{3/2})_2$
S XI-1	315.1[a]	$(1s^2\ 2s^2\ 2p_{1/2}\ 3d_{3/2})_1 \rightarrow (1s^2\ 2s^2\ 2p^2_{1/2})_0$
S XI-1	315.2[a]	$(1s^2\ 2s^2\ 2p_{3/2}\ 3d_{5/2})_2 \rightarrow (1s^2\ 2s^2\ 2p_{1/2}\ 2p_{3/2})_1$
S XI-1	315.2[a]	$(1s^2\ 2s^2\ 2p_{3/2}\ 3d_{3/2})_1 \rightarrow (1s^2\ 2s^2\ 2p^2_{3/2})_2$
S XI-2	316.1[a]	$(1s^2\ 2s2p_{1/2}\ 2p_{3/2}\ 3d_{3/2})_4 \rightarrow (1s^2\ 2s2p_{1/2}\ 2p^2_{3/2})_3$
S XI-2	316.2[a]	$(1s^2\ 2s^2\ 2p_{3/2}\ 3d_{3/2})_1 \rightarrow (1s^2\ 2s^2\ 2p_{1/2}\ 2p_{3/2})_1$
S XI-2	316.3[a]	$(1s^2\ 2s^2\ 2p_{3/2}\ 3d_{3/2})_0 \rightarrow (1s^2\ 2s^2\ 2p_{1/2}\ 2p_{3/2})_1$
S XIII-1	318.4[a]	$(1s^2\ 2s\ 3p_{3/2})_2 \rightarrow (1s^2\ 2p^2_{1/2})$
S XIII-2	327.6[a]	$(1s^2\ 2s\ 3s)_0 \rightarrow (1s^2\ 2p_{1/2}\ 2p_{3/2})_1$
S XII-1	327.4[a]	$(1s^2\ 2s2p_{1/2}\ 3d_{5/2})_{5/2} \rightarrow (1s^2\ 2s2p_{1/2}\ 2p_{3/2})_{3/2}$
S XII-1	328.6[a]	$(1s^2\ 2s2p_{3/2}\ 3d_{3/2})_{7/2} \rightarrow (1s^2\ 2s2p_{1/2}\ 2p_{3/2})_{5/2}$
S XII-2	338.2[a]	$(1s^2\ 2s^2\ 3d_{3/2})_{3/2} \rightarrow (1s^2\ 2s^2\ 2p_{3/2})_{3/2}$
S XII-2	338.3[a]	$(1s^2\ 2s^2\ 3d_{5/2})_{5/2} \rightarrow (1s^2\ 2s^2\ 2p_{3/2})_{3/2}$
S XII-2	339.8[a]	$(1s^2\ 2s^2\ 3d_{3/2})_{3/2} \rightarrow (1s^2\ 2s^2\ 2p_{1/2})_{1/2}$
S XIII-3	345.8[a]	$(1s^2\ 2s\ 3d_{5/2})_2 \rightarrow (1s^2\ 2s\ 2p_{3/2})_1$
S XII-3	357.8[a]	$(1s^2\ 2s2p_{3/2}\ 3p_{3/2})_{5/2} \rightarrow (1s^2\ 2s^2\ 2p_{3/2})_{3/2}$
S XII-3	358.3[a]	$(1s^2\ 2s2p_{1/2}\ 3p_{3/2})_{3/2} \rightarrow (1s^2\ 2s^2\ 2p_{1/2})_{1/2}$
S XIII-4	365.1[a]	$(1s^2\ 2s\ 3d_{5/2})_2 \rightarrow (1s^2\ 2s\ 2p_{1/2})_1$
S XIII-4	366.2[a]	$(1s^2\ 2s\ 3d_{3/2})_2 \rightarrow (1s^2\ 2s\ 2p_{1/2})_1$
S XIV-1	369.3[a]	$(1s^2\ 3s)_{1/2} \rightarrow (1s^2\ 2p_{3/2})_{3/2}$
S XIV-1	371.2[a]	$(1s^2\ 3s)_{1/2} \rightarrow (1s^2\ 2p_{1/2})_{1/2}$
S XII-4	376.9[a]	$(1s^2\ 2s2p_{3/2}\ 3p_{1/2})_{3/2} \rightarrow (1s^2\ 2s^2\ 2p_{3/2})_{3/2}$
S XII-4	377.2[a]	$(1s^2\ 2s2p_{3/2}\ 3p_{3/2})_{5/2} \rightarrow (1s^2\ 2s^2\ 2p_{3/2})_{3/2}$
S XIV-2	380.4[a]	$(1s^2\ 3d_{3/2})_{3/2} \rightarrow (1s^2\ 2p_{3/2})_{3/2}$

Note.
[a] Energy value from Lepson et al. (2005).

Table 2
Identified Transitions, Continued

Line/blend	Energy (eV)	Transition
S XIV-2	380.6[a]	$(1s^2\ 3d_{5/2})_{5/2} \rightarrow (1s^2\ 2p_{3/2})_{3/2}$
S XIV-2	382.2[a]	$(1s^2\ 3d_{3/2})_{3/2} \rightarrow (1s^2\ 2p_{1/2})_{1/2}$
S XIII-5	384.5[a]	$(1s^2\ 2s\ 3p_{1/2})_1 \rightarrow (1s^2\ 2s^2)_0$
S XIII-5	385.0[a]	$(1s^2\ 2s\ 3p_{3/2})_1 \rightarrow (1s^2\ 2s^2)_0$
S XI-3	397.4[a]	$(1s^2\ 2s^2\ 2p_{1/2}\ 4d_{5/2})_2 \rightarrow (1s^2\ 2s^2\ 2p_{1/2}\ 2p_{3/2})_1$
S XI-4	398.1[a]	$(1s^2\ 2s^2\ 2p_{3/2}\ 4d_{5/2})_3 \rightarrow (1s^2\ 2s^2\ 2p^2_{3/2})_2$
S XI-4	398.4[a]	$(1s^2\ 2s^2\ 2p_{3/2}\ 4d_{3/2})_2 \rightarrow (1s^2\ 2s^2\ 2p^2_{3/2})_2$
S XI-4	398.6[a]	$(1s^2\ 2s^2\ 2p_{1/2}\ 4d_{3/2})_1 \rightarrow (1s^2\ 2s^2\ 2p^2_{1/2})_0$
S XI-4	398.6[a]	$(1s^2\ 2s^2\ 2p_{3/2}\ 4d_{3/2})_2 \rightarrow (1s^2\ 2s^2\ 2p_{1/2}\ 2p_{3/2})_1$
S XIV-3	406.8[a]	$(1s^2\ 3p_{1/2})_{1/2} \rightarrow (1s^2\ 2s)_{1/2}$
S XIV-3	407.4[a]	$(1s^2\ 3p_{3/2})_{1/2} \rightarrow (1s^2\ 2s)_{1/2}$
N z	419.8[b]	$(1s\ 2s)\ ^3S_1 \rightarrow (1s^2)\ ^1S_0$
N w	430.7[b]	$(1s\ 2p)\ ^1P_1 \rightarrow (1s^2)\ ^1S_0$
S XII-5	436.8[a]	$(1s^2\ 2s^2\ 4d_{5/2})_{5/2} \rightarrow (1s^2\ 2s^2\ 2p_{3/2})_{3/2}$
S XII-6	438.4[a]	$(1s^2\ 2s^2\ 4d_{3/2})_{3/2} \rightarrow (1s^2\ 2s^2\ 2p_{1/2})_{1/2}$
S XIII-6	450.6[a]	$(1s^2\ 2s\ 4s)_0 \rightarrow (1s^2\ 2s\ 2p_{3/2})_1$
S XIII-7	457.7[a]	$(1s^2\ 2s\ 4d_{5/2})_2 \rightarrow (1s^2\ 2s\ 2p_{3/2})_1$
S XI-5	461[a]	$(1s^2\ 2s^2\ 2p\ 7d) \rightarrow (1s^2\ 2s^2\ 2p^2)^*$
S XI-6	469[a]	$(1s^2\ 2s^2\ 2p\ 8d) \rightarrow (1s^2\ 2s^2\ 2p^2)^*$
S XI-7	479[a]	$(1s^2\ 2s^2\ 2p\ 9d) \rightarrow (1s^2\ 2s^2\ 2p^2)^*$
N Ly α	500.3[c]	$(2p_{3/2})\ ^2P_{3/2} \rightarrow (1s)^2S_{1/2}$
S XIII-8	504.2[a]	$(1s^2\ 2s\ 4p_{3/2})_1 \rightarrow (1s^2\ 2s^2)_0$
S XIV-4	505.6[a]	$(1s^2\ 4s)_{1/2} \rightarrow (1s^2\ 2p)_{3/2}$

Notes.
[a] Energy value from Lepson et al. (2005).
[b] Energy value from Drake (1988).
[c] Energy value from Garcia & Mack (1965).

spectrum. The measured ratios in Table 5 show that its strength is about 59% of the intensity of the $3p \rightarrow 2s$ line at 407 eV in the CX spectrum. The corresponding percentage in the direct-excitation spectrum is only about 3.7%. The transitions from $n_c = 7, 8$ show similar enhancements in CX.

Another telling feature of the CX spectrum is the change in the $n = 3 \rightarrow n = 2$ transitions between 369 and 407 eV. The $3s \rightarrow 2p$ (S XIV-1) and $3p \rightarrow 2s$ (S XIV-3) transitions are significantly enhanced compared to the $3d \rightarrow 2p$ (S XIV-2) peak. In the overlaid spectrum in Figure 2, it can be seen that the blended $3d \rightarrow 2p$ peak at about 380 eV slightly shifts toward lower energy in the CX spectrum. The $3d \rightarrow 2p$ lines of S XIV are blended with S XIII lines. It appears that the $3p \rightarrow 2s$ transitions in S XIII (S XIII-5) get weaker in CX, which would account for the shift.

The beryllium-like, boron-like, and carbon-like sulfur lines all show a similar pattern as their lithium-like counterparts. Again, there is a strong enhancement in the $n_c = 7, 8, 9 \rightarrow n = 2$ levels transitions. Generally, the principal quantum number n_c into which an electron is preferentially captured slightly decreases as a function of decreasing charge state, which can be seen in Figures 2–4. The $n = 3 \rightarrow n = 2$ lines of S XI are between 314 and 316 eV. The lines are marked S XI-1 and S XI-2 in the blended peak. The S XI lines emanating from levels of electron capture, n_c, are situated between 460 and 480 eV and are marked as S XI-5, S XI-6, S XI-7 in the graphs. These lines show a significant

Table 3
Identified Transitions, Continued

Line/blend	Energy (eV)	Transition
S XIV-5	510.3[a]	$(1s^2\ 4d)_{5/2} \rightarrow (1s^2\ 2p)_{3/2}$
S XIII-8	509.6[a]	$(1s^2\ 2s\ 5d_{5/2})_2 \rightarrow (1s^2\ 2s\ 2p_{3/2})_1$
S XIV-6	512.1[a]	$(1s^2\ 4d)_{3/2} \rightarrow (1s^2\ 2P)_{1/2}$
S XII-8	523[e]	$(1s^2\ 2s^2\ 7d) \rightarrow (1s^2\ 2s^2\ 2p)$
S XII-9	532[e]	$(1s^2\ 2s^2\ 8d) \rightarrow (1s^2\ 2s^2\ 2p)$
S XII-10	537[e]	$(1s^2\ 2s^2\ 9d) \rightarrow (1s^2\ 2s^2\ 2p)$
S XIV-7	538.6[a]	$(1s^2\ 4p)_{1/2} \rightarrow (1s^2\ 2s)_{1/2}$
S XIV-7	538.8[a]	$(1s^2\ 4p)_{3/2} \rightarrow (1s^2\ 2s)_{1/2}$
S XIII-9	552[e]	$(1s^2\ 2s\ 7d) \rightarrow (1s^2\ 2s\ 2p_{3/2})$
S XIII-10	558.2[a]	$(1s^2\ 2s\ 5p_{3/2})_1 \rightarrow (1s^2\ 2s^2)_0$
S XIII-10	559[e]	$(1s^2\ 2s\ 6d) \rightarrow (1s^2\ 2s\ 2p)$
S XIII-10	559[e]	$(1s^2\ 2s\ 6s) \rightarrow (1s^2\ 2s\ 2p)$
O z	561.9[b]	$(1s\ 2s)^3S_1 \rightarrow (1s^2)^1S_0$
S XIII-11	565[e]	$(1s^2\ 2s\ 8d) \rightarrow (1s^2\ 2s\ 2p)$
S XIV-8	570 [a]	$(1s^2\ 5s)_{1/2} \rightarrow (1s^2\ 2p)_{1/2}$
S XIV-8	570[a]	$(1s^2\ 5s)_{1/2} \rightarrow (1s^2\ 2p)_{3/2}$
S XIV-8	570.3[a]	$(1s^2\ 5d)_{5/2} \rightarrow (1s^2\ 2p)_{3/2}$
O y	568.7[b]	$(1s\ 2p)^3P_1 \rightarrow (1s^2)^1S_0$
S XIII-12	573[e]	$(1s^2\ 2s\ 9d) \rightarrow (1s^2\ 2s\ 2p_{3/2})$
O w	573.9[b]	$(1s\ 2p)\ ^1P_1 \rightarrow (1s^2)^1S_0$
S XIII-13	579[e]	$(1s^2\ 2s\ 7d) \rightarrow (1s^2\ 2s\ 2p_{1/2})$
S XIII-13	579[e]	$(1s^2\ 2s\ 7s) \rightarrow (1s^2\ 2s\ 2p)$
S XIII-14	590[e]	$(1s^2\ 2s\ 8d) \rightarrow (1s^2\ 2s\ 2p_{1/2})$

Notes.
[a] Energy value from Lepson et al. (2005).
[b] Energy value from Drake (1988).
[e] Energy value from present GRASP calculations.

Table 4
Identified Transitions, Continued

Line/blend	Energy (eV)	Transition
S XIII-14	590[e]	$(1s^2\ 2s\ 8s) \rightarrow (1s^2\ 2s\ 2p)$
N Ly β	592.9[c]	$(3p)^2P_{3/2} \rightarrow (1s)^2S_{1/2}$
S XIII-15	598[e]	$(1s^2\ 2s\ 9d) \rightarrow (1s^2\ 2s\ 2p_{1/2})$
S XIII-15	598[e]	$(1s^2\ 2s\ 9s) \rightarrow (1s^2\ 2s\ 2p)$
S XIII-15	599[e]	$(1s^2\ 2s\ 7p) \rightarrow (1s^2\ 2s^2)$
S XIV-9	598[a]	$(1s^2\ 5p_{3/2})_{3/2} \rightarrow (1s^2\ 2s)_{1/2}$
S XIV-9	598[a]	$(1s^2\ 5p_{1/2})_{1/2} \rightarrow (1s^2\ 2s)_{1/2}$
S XIV-9	604[e]	$(1s^2\ 6d) \rightarrow (1s^2\ 2p)$
S XIV-9	604[e]	$(1s^2\ 6s) \rightarrow (1s^2\ 2p)$
S XIII-16	609[e]	$(1s^2\ 2s\ 8p) \rightarrow (1s^2\ 2s^2)$
S XIII-17	599[e]	$(1s^2\ 2s\ 9p) \rightarrow (1s^2\ 2s^2)$
S XIV-10	624[e]	$(1s^2\ 7d) \rightarrow (1s^2\ 2p)$
S XIV-10	624[e]	$(1s^2\ 7s) \rightarrow (1s^2\ 2p)$
S XIV-11	633[e]	$(1s^2\ 6p) \rightarrow (1s^2\ 2s)$
S XIV-12	638[e]	$(1s^2\ 8d) \rightarrow (1s^2\ 2p)$
S XIV-12	638[e]	$(1s^2\ 8s) \rightarrow (1s^2\ 2p)$
S XIV-13	644[e]	$(1s^2\ 9d) \rightarrow (1s^2\ 2p)$
S XIV-13	644[e]	$(1s^2\ 9s) \rightarrow (1s^2\ 2p)$
S XIV-14	652[e]	$(1s^2\ 7p) \rightarrow (1s^2\ 2s)$
O Ly α	653.9[c]	$(2p)^1P_{3/2} \rightarrow (1s)^2S_{1/2}$
S XIV-15	664[e]	$(1s^2\ 8p) \rightarrow (1s^2\ 2s)$
O K β	665.6[d]	$(3p)^2P_{3/2} \rightarrow (1s)^2S_{1/2}$
S XIV-16	675[e]	$(1s^2\ 9p) \rightarrow (1s^2\ 2s)$

Notes.
[c] Energy value from Garcia & Mack (1965).
[d] Energy value from Vainshtein & Safronova (1985).
[e] Energy value from present GRASP calculations.

enhancement when excited by CX, whereas the $n = 3 \rightarrow n = 2$ lines get comparatively weaker. These changes can be observed in the overlaid spectra in Figure 2. The measured ratios of the CX and direct-excitation emissions in specific lines are listed in Table 5, which shows that the intensity of the high-n line S XI-6 (transitions from $n = 8$) is about 49% of the intensity of the SXI-1, 2 feature when produced by CX, whereas this ratio is only about 4.2% in the direct excitation spectrum. These ratios are similar to the ones observed in S XIV.

Table 5
Intensity Ratios for Selected Transitions Produced by CX and Direct Excitation in the Highest (S XIV) and Lowest (S XI) Charge States in the Observed Spectra

Peak Ratio	Direct Excitation	Charge Exchange
$\frac{\text{counts(S XIV}-13)}{\text{counts(S XIV}-3)}$	0.042 ± 0.0012[a]	0.49 ± 0.032[a]
$\frac{\text{counts(S XI}-6)}{\text{counts(S XI}-1,2)}$	0.037 ± 0.0013[a]	0.59 ± 0.081[a]

Notes. The ratios consist of the strongest high-n lines and the strongest $n = 3 \rightarrow n = 2$ transitions in the respective charge states and have been corrected for the ECS filter absorption.
[a] Errors are purely statistical.

4. DISCUSSION AND COMPARISON WITH JOVIAN OBSERVATIONS

The energy level having the largest probability of being populated in a charge transfer process can be approximated by Janev & Winter (1985)

$$n_c \approx q \left(\frac{I_{\rm H}}{I_n}\right)^{1/2} \left(1 + \frac{q-1}{\sqrt{2q}}\right)^{-1/2}, \quad (1)$$

where q is the ion charge, I_n is the ionization potential of the neutral species, and $I_{\rm H}$ is the ionization energy for hydrogen. For S^{+14} ions recombining with neutral SF_6 gas ($I_{SF_6} \approx 15.9$ eV), this gives $n_c \approx 8$. The approximation roughly agrees with our results, where we see electron capture into $n_c = 7$, 8, and 9, although mostly to $n_c = 9$.

As mentioned before, L-shell CX spectra have not yet been modeled. However, some general predictions can be made based on the angular momentum of the state into which the electron is captured. The angular momentum state, l, in large part determines how the electron can decay, due to the selection rule $\Delta l = \pm 1$ for electric dipole transitions. In the $n = 2$ state of L-shell sulfur, there are both $l = 0$ and $l = 1$ angular momentum states. Hence, if an electron were captured in an s, p, or d-state, direct decay to $n = 2$ would be possible. In this case we would detect the transitions n_c (s, p, d) $\rightarrow$ 2 (s, p). Such low-l states usually get populated at low-collision energies (Ryufuku & Watanabe 1979). For charge transfer to higher l states in n_c, the electron needs to decay by cascades, which changes its l value by unity for every step in the radiative cascade. Finally, the electron would end up in the $n = 3$, 4, 5, or 6 states and the transitions $n = 3, 4, 5, 6 \rightarrow n = 2$ would be enhanced (Wargelin et al. 2005). Another possible process in CX reactions is double-electron capture. This is followed by autoionization, where one electron drops to a lower n level while the other gets ionized (Ali et al. 2005). If this occurs, one would see an enhancement in the flux from that lower n level, e.g., $n = 3, 4, 5, 6 \rightarrow n = 2$ (Beiersdorfer et al. 2008).

Because we observe the strongest enhancement in the $n_c \rightarrow n = 2$ transitions, we can conclude that mainly low-l levels were populated in the charge exchange. This is in agreement with the low ion temperature in EBIT, about 10–20 eV amu^{-1}, which provides the low-collision energies that favor the population of low-l states during CX (Beiersdorfer et al. 2000). It also suggests

that high-l capture into n_c followed by cascades, which is mainly a result of high-collision energy, is less likely than double-electron capture, as the fraction of double-electron captures can approach almost half of the total (Ali et al. 2005). However, detailed radiative cascade models are needed to discern which of these processes is more probable.

The low-energy part of the Jovian auroral X-ray emission measured by *Chandra* and *XMM-Newton* is thought to be due to L-shell sulfur CX (Elsner et al. 2005; Cravens et al. 2003; Branduardi-Raymont et al. 2007; Kharchenko et al. 2006). To infer the ionic source of the X-ray emission, spectral fits using the VAPEC model were made by Elsner et al. (2005). VAPEC is a collisional equilibrium model used mainly for studying astrophysical plasmas and uses updated line intensity data to create the fits. For Jupiter's auroral emission, fits were made using a sulfur–oxygen plasma and a carbon–oxygen plasma. Runs were made for sulfur (or carbon) and oxygen at different temperatures and combined in order to fit the *Chandra* spectrum. The sulfur–oxygen model was found to be a better fit than the carbon–oxygen model. In this fit, the oxygen model presumes a temperature of 335 eV and the sulfur model presumes a temperature of 172 eV. These temperatures are not physical, but can be understood as corresponding to specific charge states (Elsner et al. 2005). A sulfur temperature of 172 eV would correspond to a charge state dominated by S^{10+}. The suggestion of S XI as being responsible for the 300 eV emission was supported by the analysis of the peak in three *XMM* spectra, where centroid energies of 0.30, 0.31, 0.32 keV were determined. This is consistent with the emission from S XI, which the authors predicted to peak at 0.32 keV and with S XII, predicted to peak at 0.34 keV (Branduardi-Raymont et al. 2007). However, it is quite inconsistent with the emission from carbon since the C VI emission peaks at 0.37 keV. Also some Monte Carlo simulations of ion fluxes of sulfur and oxygen ions have been made using collision cross sections for stripping, electron capture and target ionization (Kharchenko et al. 2006). The results are found to be in reasonable agreement with the *Chandra* and *XMM-Newton* observations, further supporting the magnetospheric origin theory (Kharchenko et al. 2006).

The energy that our measurement was carried out at produced a higher charge state distribution than the one in the VAPEC model, but S XI lines are nevertheless visible in our spectra. In direct excitation, the strongest lines, the $n = 3 \rightarrow n = 2$ transitions, are at 314–316 eV. The $n_c \rightarrow n = 2$ CX lines for S XI were found between 460 and 480 eV in our measurement. Thus, for a CX spectrum with a charge balance of mainly S XI, lines due to electron capture into n_c should be observed in this area. However, there is an apparent lack of lines in the *Chandra* spectrum between 400 and 500 eV (Elsner et al. 2005). This absence of emission suggests that L-shell sulfur CX, as produced in our laboratory experiments, may not adequately explain the shape of the *Chandra* spectra.

It should be noted that the VAPEC model produces a low-energy collisional spectrum, whereas the Jupiter spectrum is thought to be produced by CX-collisions at very high energy (on the order of MeV) (Kharchenko et al. 2006). Our measurements were performed at low-collision energy (10–20 eV amu^{-1}). As the collision energy increases, the peaks due to transitions from n_c will diminish (Ryufuku & Watanabe 1979; Perez et al. 2005; Beiersdorfer et al. 2001). Thus, at the high collision energies thought to prevail in the Jupiter plasma, the chance of capturing the electrons into low-l states is reduced. The ions may in large part decay through cascades from high-l states, which may make the peaks due to transitions from n_c too weak to observe in the Jupiter spectra. Another explanation might be that L-shell sulfur CX is not responsible for the emission, or that collisional excitation of sulfur ions dominates the emission. Indeed, the Jovian spectra resemble more closely the laboratory spectra formed by electron collisions. Jovian spectra recorded with higher resolution and additional laboratory-produced spectra of sulfur at lower energy may be helpful in shedding light on this problem.

Beiersdorfer et al. (2008) collected moderate resolution L-shell CX spectra of iron. They discovered that the enhancement in the CX spectra was stronger in the transitions $n = 4, 5 \rightarrow n = 2$ than in the $n_c \rightarrow n = 2$ transitions. In the CX-induced spectrum of lithium-like sulfur, the enhancement in the $n_c \rightarrow n = 2$ transitions was almost a factor of 20 when compared with the $3p \rightarrow 2s$ transitions. In lithium-like iron this enhancement was only around a factor of 3.5 when compared with the $n = 3 \rightarrow n = 2$ blended peak (Beiersdorfer et al. 2008). The reason for this difference can probably be traced to the moderate resolution of the detector used in the iron measurement, which smeared out the peak intensity and made the analysis more uncertain. However, just as for sulfur, the enhanced emission from $n = 4$ and 5 could either be populated by single electron capture into n_c followed by cascades down to $n = 4$ and 5 or by double electron capture followed by autoionization where one electron drops to $n = 4, 5$. Since in iron the enhancement in transitions from levels $n < n_c$ is stronger than the enhancement in transitions from n_c, it could mean that double electron capture was more prevalent in the iron measurement than in the present sulfur measurement.

Another feature that was discovered in the iron measurement was a shift in energy of the $n = 3 \rightarrow n = 2$ peak: The $n = 3 \rightarrow n = 2$ peak (around 0.9 keV) was seen to be slightly shifted toward lower energy when produced by CX. It was proposed that this shift could be due to an enhancement in the $3s \rightarrow 2p$ transitions, since it is lowest in energy among the $n = 3 \rightarrow n = 2$ transitions. However, because of possible changes in the ionization balance in CX versus direct excitation, it was not known if this shift was significant (Beiersdorfer 2008). In our sulfur measurement, we had improved spectral resolution, and thus much less blending of the lines from different charge states. In the sulfur spectra, most transitions in the $n = 3 \rightarrow n = 2$ peak are resolved. Although the intensity of the $3s \rightarrow 2p$ transitions is enhanced when formed by CX, the $3p \rightarrow 2s$ peak also shows a significant enhancement. Furthermore, the $3d \rightarrow 2p$ blend (with S XIII) slightly shifts to lower energy. This is the result of a decrease in the $3p \rightarrow 2s$ transitions in S XIII and would mean that the centroid energy of the $n = 3 \rightarrow n = 2$ transitions in lithium-like sulfur has also shifted toward lower energy. This shift of the $n = 3 \rightarrow n = 2$ peak, as seen in both the lithium-like sulfur and the iron measurements, could possibly be a diagnostic for L-shell CX. However, the changes in intensity of the resolved, individual $n = 3 \rightarrow n = 2$ transitions for all the recorded charge states show no consistent behavior in CX. More L-shell CX data are needed to examine the possibility of an $n = 3 \rightarrow n = 2$ peak L-shell CX diagnostic.

5. SUMMARY

The results presented from our sulfur L-shell measurements are the first to report on individual transitions formed by charge exchange. In the CX spectra, we found a significant enhancement in the transitions $n = 4, 5, 6 \rightarrow n = 2$, in

comparison with the $n = 3 \rightarrow n = 2$ transitions that dominate direct excitation. An even greater enhancement was recorded in the transitions from levels of electron capture $n_c = 7, 8, 9 \rightarrow n = 2$. The spectra mainly consisted of S XIV, but lower charge states such as S XIII, S XII, and S XI also contribute. These lower charge states show a very similar pattern to the S XIV emission in CX.

The results have been compared to the peak around 300 eV in the spectra from the Jovian polar regions, observed by the *Chandra* and *XMM-Newton* satellites. This peak is believed to result from L-shell CX emission in mainly carbon-like sulfur. However, the peak in the spectra from Jupiter's aurora and the S XI emission from EBIT do not match. This means that we cannot yet conclude that CX produced the 300 eV peak. In fact, CX may not be the correct mechanism underlying X-ray production on Jupiter's polar regions. The $n_c = 7, 8, 9 \rightarrow n = 2$ lines in S XI between 460 and 480 eV, which are diagnostic of charge exchange, are not seen in the *Chandra* spectra. This absence might be due to the difference in the fundamental conditions affecting CX in both sources, such as ion temperature, collision energy, and neutral gas composition. But it remains to be seen whether these differences suffice to explain the mismatch.

Work at LLNL was performed under the auspices of the U.S. Department of Energy by Lawrence Livermore National Laboratory under Contract DE-AC52-07NA27344 and was in part supported by NASA, including through grant NNG06GB11G from the Planetary Atmospheres Program to UC Berkeley and through support from the Astronomy and Physics Research and Analysis Program received by LLNL, SAO, and GSFC. Part of the work was funded by the Laboratory Directed Research and Development Program at LLNL under project tracking number 06-ERD-010.

M. F. would like to thank Prof. Tomas Brage as well as Dr. P.O. Zetterberg and Dr. Carl-Erik Magnusson at Lund University, Lund, Sweden, for their continued support during her stay at Livermore. The authors wish to thank Joel Clementson, Daniel Thorn, and Ed Magee for their technical support and advice.

REFERENCES

Ali, R., Neill, P. A., Beiersdorfer, P., Harris, C. L., Rakovi, M. J., Wang, J. G., Schultz, D. R., & Stancil, P. C. 2005, ApJ, 629, 125
Allen, F. I., Biedermann, C., Radtke, R., & Fussmann, G. 2007, J. Phys., Conf. Ser., 58, 188
Beiersdorfer, P. 2008, Can. J. Phys., 86, 1
Beiersdorfer, P., et al. 2003, Nucl. Instrum. Methods Phys. Res. B, 205, 173
Beiersdorfer, P., Bitter, M., Olson, R., & Marion, M. 2005a, Phys. Rev. A, 72, 032725
Beiersdorfer, P., Chen, H., Boyce, K. R., Brown, G. V., Kelley, R. L., Kilbourne, C. A., Porter, F. S., & Kahn, S. M. 2005b, Nucl. Instrum. Methods, 235, 116
Beiersdorfer, P., Lisse, C. M., Olson, R. E., Brown, G. V., & Chen, H. 2001, ApJ, 549, L147
Beiersdorfer, P., et al. 2000, Phys. Rev. Lett., 85, 5090
Beiersdorfer, P., Schweikhard, L., Crespo Lopez-Urrutia, J., & Widmann, K. 1996, Rev. Sci. Instrum., 67, 3818
Beiersdorfer, P., Schweikhard, L., Liebisch, P., & Brown, G. V. 2008, ApJ, 672, 726
Bhardwaj, A., et al. 2007, Planet. Space Sci., 55, 1135
Branduardi-Raymont, G., et al. 2007, A&A, 463, 761
Branduardi-Raymont, G., Elsner, R. F., Gladstone, G. R., Ramsay, G., Rodriguez, P., Soria, R., & Waite, J. H., Jr. 2004, A&A, 424, 331
Bunce, E. J., Cowley, S. W. H., & Yeoman, T. K. 2004, J. Geophys. Res., 109, A09S13
Cox, D. P. 1998, in The Local Bubble and Beyond, ed. D. Breitschwerdt, M. J. Freyberg, & J. Trümper (New York: Springer), 121
Cravens, T. E. 2000, ApJ, 532, L153
Cravens, T. E., Robertson, I. P., & Snowden, S. L. 2001, J. Geophys. Res., 106, 24883
Cravens, T. E., Waite, J. H., Gombosi, T. I., Lugaz, N., Gladstone, G. R., Mauk, B. H., & MacDowall, R. J. 2003, J. Geophys. Res., 108, 25
Drake, G. W. 1988, Can. J. Phys., 66, 586
Elsner, R. F., et al. 2005, J. Geophys. Res., 110, 1
Fujimoto, R., et al. 2007, PASJ, 59, 133
Garcia, J. D., & Mack, J. E. 1965, J. Opt. Soc. Am., 55, 654
Janev, R. K., & Winter, H. 1985, Phys. Rep., 117, 265
Kharchenko, V., & Dalgarno, A. 2001, ApJ, 554, L99
Kharchenko, V., Dalgarno, A., Schultz, D. R., & Stancil, P. C. 2006, Geophys. Res. Lett., 33, L11105
Kharchenko, V., Rigazio, M., Dalgarno, A., & Krasnopolsky, V. A. 2003, ApJ, 585, L73
Lepson, J. K., Beiersdorfer, P., Behar, E., & Kahn, S. M. 2005, ApJ, 625, 1045
Marrs, R. 2008, Can. J. Phys., 86, 11
McCammon, D., et al. 2002, ApJ, 576, 188
Olsen, R. E. 1981, Phys. Rev. A, 24, 1726
Otranto, S., Olson, R. E., & Beiersdorfer, P. 2006, Phys. Rev. A, 73, 022723
Parpia, F. A., Froese Fischer, C., & Grant, I. P. 1996, Comput. Phys. Commun., 94, 249
Perez, J. A., & Olson, R. E. 2005, Nucl. Instrum. Methods Phys. Res. B, 241, 134
Porter, F. S., et al. 2008, Can. J. Phys., 86, 231
Ryufuku, H., & Watanabe, T. 1979, Phys. Rev. A, 20, 1828
Sanders, W. T., Edgar, R. J., Kraushaar, W. L., McCammon, D., & Morgenthaler, J. P. 2001, ApJ, 554, 694
Schwadron, N. A., & Cravens, T. E. 2000, ApJ, 544, 558
Snowden, S. L., McCammon, D., Burrows, D. N., & Mendenhall, J. A. 1994, ApJ, 424, 714
Vainshtein, L. A., & Safrona, U. I. 1985, Physica Scripta, 31, 519
Wargelin, B. J., Beiersdorfer, P., & Brown, G. V. 2008, Can. J. Phys., 86, 151
Wargelin, B. J., Beiersdorfer, P., Neill, P. A., Olson, R. E., & Scofield, J. H. 2005, ApJ, 634, 687